Electronic Supplementary Material (ESI) for Energy & Environmental Science.

Suppressing the energetic disorder of all-polymer solar cells enables over 18% efficiency

Tao Zhang,[a,b] Ye Xu, [a,f] Huifeng Yao,*[a] Jianqi Zhang,[c] Pengqing Bi, [a] Zhihao Chen, [a] Jingwen Wang, [a,b] Yong Cui,[a] Lijiao Ma,[a] Kaihu Xian,[e] Zi Li, [a] Xiaotao Hao, [d] Zhixiang Wei [c] and Jianhui Hou*[a,b]

[a] State Key Laboratory of Polymer Physics and Chemistry, Beijing National Laboratory for Molecular Sciences, CAS Research/Education Center for Excellence in Molecular Sciences, Institute of Chemistry, Chinese Academy of Sciences,100190 Beijing, PR China.

[b] University of Chinese Academy of Sciences, 100049 Beijing, PR China.

[c] CAS key laboratory of nanosystem and hierarchical fabrication, CAS Center for Excellence in Nanoscience, National Center for Nanoscience and Technology, 100190 Beijing, China.

[d] School of Physics, State Key Laboratory of Crystal Materials, Shandong University, Jinan, Shandong 250100, P. R. China.

[e] School of Materials Science and Engineering, Tianjin Key Laboratory of Molecular Optoelectronic Sciences, Tianjin University, and Collaborative Innovation Center of Chemical Science and Engineering (Tianjin), Tianjin 300350, P. R. China.

[f] State Key Laboratory of Photovoltaic Science and Technology, Trina Solar, Changzhou, 213031 China.

Instruments and Measurements

^{1}H NMR and ^{13}C NMR spectra were recorded in deuterated solvents on a Bruker DPX 300 or 400. Elemental analysis was performed on an instrument of Flash EA1112. Density functional theory (DFT) calculations were carried out using the level of B3LYP/6-31G(d,p). The UV-vis absorption spectroscopy measurements were conducted on a Hitachi UH4150 spectrophotometer. Electrochemical cyclic voltammetry measurements were performed on a CHI650D electrochemical workstation with a three-electrode system. Pt wire and glassy carbon electrode were used as the counter electrode and working electrode, respectively. Ag/Ag^{+} was used as the reference electrode, and the ferrocene/ferrocenium redox couple (Fc/Fc^{+}) was used as the internal calibration. Ultraviolet photoelectron spectroscopy (UPS) was measured by using Thermo Scientific ESCALAB 250Xi with a He-discharged lamp. The *J*−*V* measurements were performed by using the solar simulator (SS-F5-3A, Enlitech) along with AM 1.5G spectra (100 mW/cm^{2}). The EQE spectra were measured through the Solar Cell Spectral Response Measurement System QE-R3011 (Enli Technology Co., Ltd., Taiwan). The emission spectra and light intensity of the LED light sources were measured by a Fiber Optics Spectrometer (Maya2000 Pro, Ocean Optics). The photoinduced charge extraction by linearly increasing voltage (photo-CELIV) measurement was performed by the all-in-one characterization platform Paios developed and commercialized by Fluxim AG, Switzerland. In order to reflect the true information, all of the organic photovoltaic cells (OPV cells) are prepared for photo-CELIV measurements according to the corresponding device fabrication conditions. Ramp Rate: 0.10 V/us; Delay Time: 70 us; Light-Pulse Length: 30 us; Setup-Type: LED. Highly Sensitive EQE (*s*-EQE) was measured by using an integrated system (PECT-600, Enlitech), where the photocurrent was amplified and modulated by a lock-in instrument. Electroluminescence (EL) quantum efficiency (EQE_{EL}) measurements were performed by applying external voltage/current sources through the OPV cells (ELCT-3010, Enlitech). AFM height and phase images were recorded on a Nanoscope AFM microscope (Bruker), where the tapping mode was used. The samples were fabricated in accordance with the conditions of the best OPV cells. The EQE mapping measurements were carried out by using LSD4 system (Enlitech). The instrument is equipped with 405 and 520 nm lasers. Considering the OPV cells have high EQE values around 520 nm, we select 520 nm laser under the test. Grazing incidence wide-angle X-ray scattering (GIWAXS) measurements were performed on a XEUSS SAXS/WAXS system (XENOCS, France) at the National Center for Nanoscience and Technology (NCNST, Beijing). Femtosecond transient absorption spectroscopy was measured on an Ultrafast Helios pump-probe system in collaboration with a regenerative amplified laser system from Coherent. An 800 nm pulse with a repetition rate of 1kHz, a length of 100 fs, and an energy of 7 mJ/pluse, was generated by a Ti:sapphire amplifier (Astrella, Coherent). Then the 800 nm pulse was separated into two parts by a beam splitter. One part was coupled into an optical parametric amplifier (TOPAS, Coherent) to generate the pump pulses at 400 and 800 nm. The other part was focused onto a sapphire plate and a YAG plate to generate white light supercontinuum as the probe beams with spectra covering 420-800

nm and 750-1600 nm, respectively. The time delay between the pump and probe was controlled by a motorized optical delay line with a maximum delay time of 8 ns. The sample films were spin-coated onto the 1 mm-thick quartz plates and encapsulated by epoxy resin in a nitrogen-filled glove box to resist water and oxygen in the air. The pump pulse is chopped by a mechanical chopper with 500 Hz and then focused on the mounted sample with probe beams. The probe beam was collimated and focused into a fiber-coupled multichannel spectrometer with CCD sensor. The energy of pump pulse was measured and calibrated by a power meter (PM400, Thorlabs). Molecular weight and molecular weight distribution were measured by high-temperature size-exclusion chromatography (HT-SEC) coupled with triple detectors (PL-GPC220 at 150 °C, with 1,2,4-trichlorobenzene as the solvent). The chromatographic system consisted of a Polymer Labs PL 220 HT-SEC with a two-angle laser light scattering (LS) detector, a viscometer detector (VD) and a differential refractive index (DRI) detector.

Device fabrication

Fabrication of the OPV cell via a spin-coating method. OPV cells were fabricated with the conventional device structure (glass/ITO/PEDOT:PSS/active layers/PNINN/Ag). The ITO-coated glass was purchased from South China Xiang's Science & Technical Company Limited. PEDOT:PSS (4083) was purchased from the Clevios™. PY-IT and PDINN were purchased from Solarmer Material Inc. PEDOT:PSS was diluted with the same volume of water. PDINN was dissolved in methanol at a concentration of 1.5 mg/ml. PBQx-TF/PQB-1/PQB-2/PQB-3/PBDB-TF:PY-IT with weight ratio of 1:1 were dissolved in toluene at the polymer concentration of 6 mg/mL. The solutions need to be stirred at 80˚C until completely dissolved. Before spin-coating the active layer, 2% 1-Chloronaphthalene (v/v) was added to the solutions. All PSCs were fabricated by the following conditions: Firstly, about 10 nm PEDOT:PSS layers were spin-coated on the pre-cleaned ITO substrates and annealed at 150°C for 15 min. Subsequently, the substrates were transferred to the nitrogen glove box. The mixed solutions were spin-coated onto the PEDOT:PSS layers, and then the films were treated with thermal annealing at 100˚C for 10 min. The best active layer thickness is about 100 nm. PDINN was spin-coated on the top of the active layers at 3000 rpm for 30 s. Finally, 150 nm Ag was deposited under a high vacuum. In our laboratory, the areas of the masks are about 0.062 cm^2.

Charge transport properties. The hole mobility was measured by the SCLC method, employing a device architecture of ITO/PEDOT:PSS /polymers /Au.

Synthetic detail

Scheme S1. The synthetic route of three polymers.

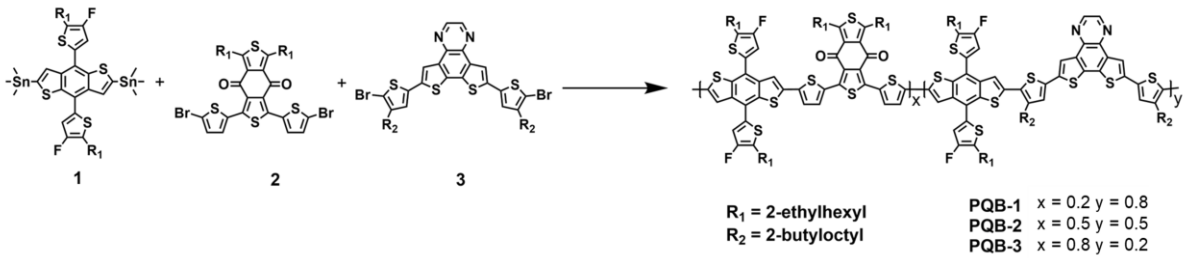

Synthesis of PQB-1, PQB-2, and PQB-3.

The synthesis procedures of compouds 2 and 3 are based on our previous works. [1,2] 0.2 mmol Compound 1, 0.2 mmol bromide monomer (0.04 mmol compound 2/0.16 mmol compound 3, 0.1 mmol compound 2/0.1 mmol compound 3, 0.16 mmol compound 2/0.04 mmol compound 3), 0.003 mmol $Pd_2(dba)_3$ and 0.03 mmol $P(o\text{-}tol)_3$ was added to 8 mL toluene. The polymerization reaction was heated at 120 ℃ for 2 hours under the protection of argon. After cooling to room temperature, the polymer material was precipitated in methanol (60 mL). The precipitates were dried and purified by flash silica gel column chromatography by using hot chlorobenzene as eluent. The polymer was obtained by reprecipitating the chlorobenzene solution in methanol. The solid was filtered and dried under vacuum for 24 h before use. The yields of PQB-1, PQB-2 and PQB-3 are 50%, 57%, and 53%, respectively.

Elemental analysis calcd (%) for PQB-1 ($C_{76}H_{92.4}F_2O_{0.4}N_{1.6}S_8$): C = 68.7%, H = 6.96%, N = 1.69%. Found: C = 68.5%, H = 6.88%, N = 1.57%.

Elemental analysis calcd (%) for PQB-2 ($C_{73}H_{85}F_2ONS_8$): C = 68.2%, H = 6.61%, N = 1.09%.

Found: C = 67.78%, H = 6.66%, N = 0.98%.

Elemental analysis calcd (%) for PQB-3 ($C_{70}H_{79.6}F_2O_{1.6}N_{0.4}S_8$): C = 67.5%, H = 6.39%, N = 0.45%. Found: C = 67.11%, H = 6.40%, N = 0.37%.

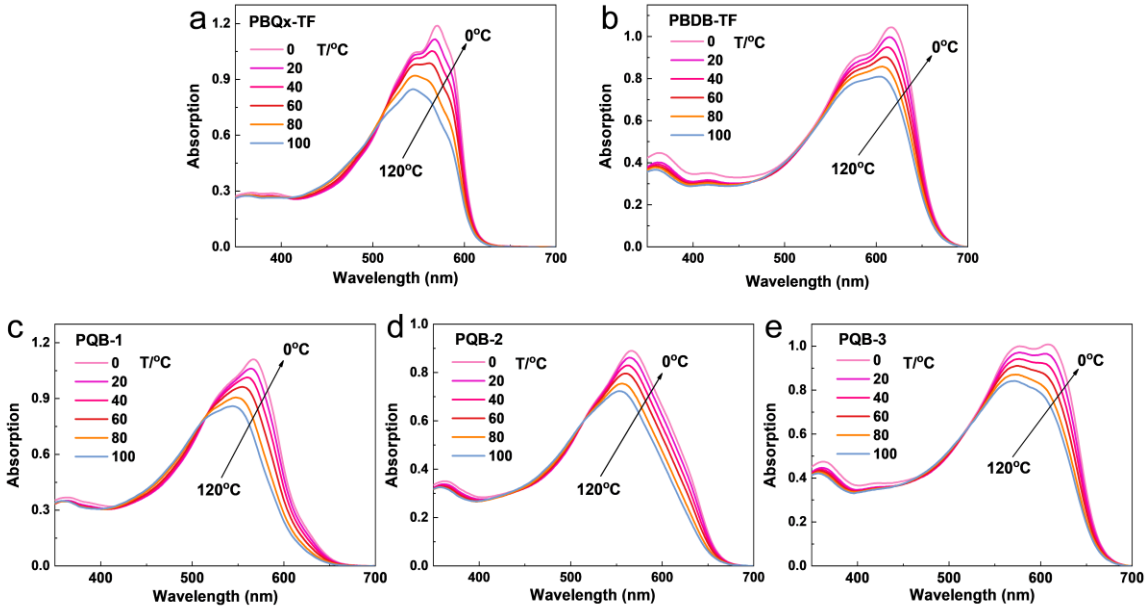

Figure S1. The temperature-dependent absorption spectra of (a) PBQx-TF, (b) PBDB-TF, (c) PQB-1, (d) PQB-2 and (e)PQB-3 in toluene solution.

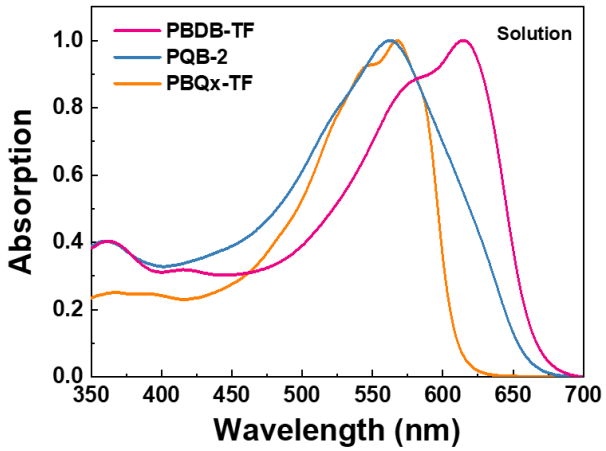

Figure S2. The absorption spectra of PBDB-TF, PQB-2 and PBQx-TF in toluene solution.

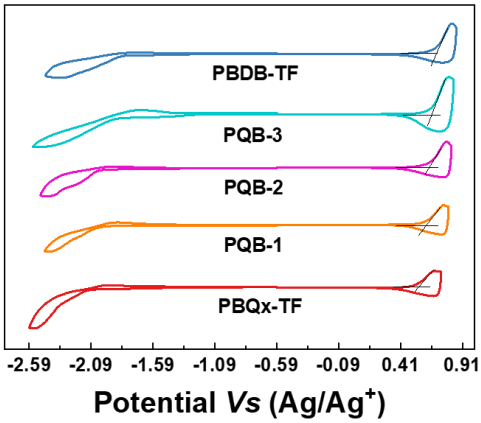

Figure S3. Cyclic voltammetry curves of polymers.

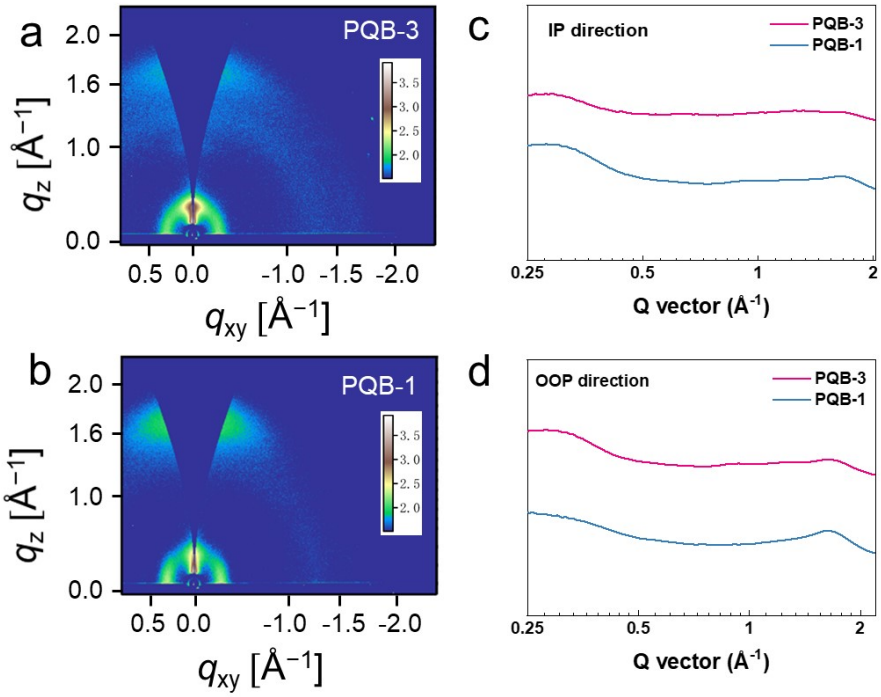

Figure S4. (a,b) 2D-GIWAXS patterns of PQB-3 and PQB-1 films. (c,d) The GIWAXS profiles of PQB-3 and PQB-1 films in IP and OOP directions.

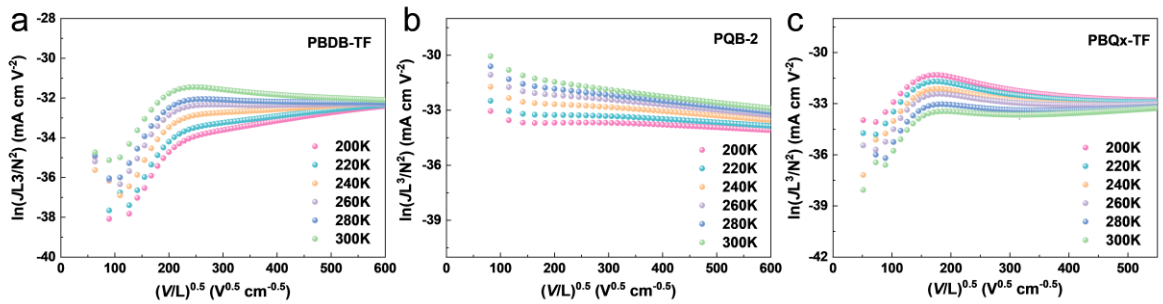

Figure S5. SCLC plots under different temperatures for (a) PBDB-TF, (b) PQB-2, and (c) PBQx-TF-based devices.

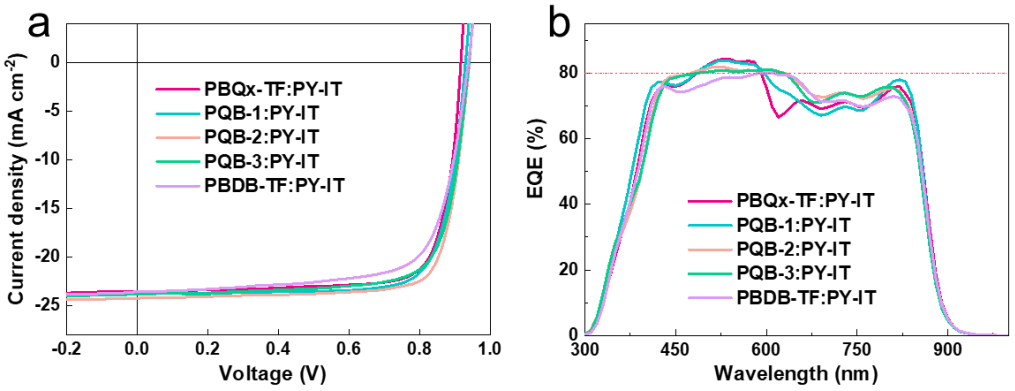

Figure S6. (a) *J-V* and (b) EQE curves in AM 1.5G of all PSCs.

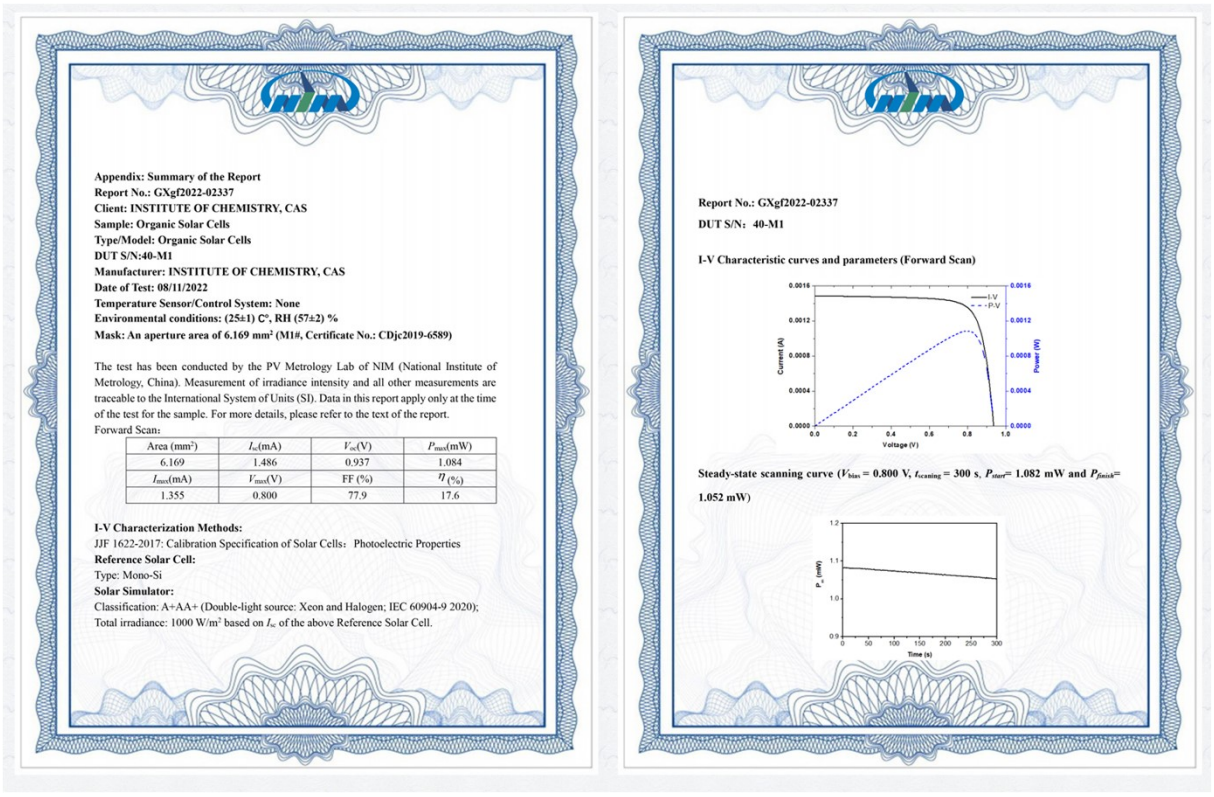

Appendix: Summary of the Report
Report No.: GXgf2022-02337
Client: INSTITUTE OF CHEMISTRY, CAS
Sample: Organic Solar Cells
Type/Model: Organic Solar Cells
DUT S/N:40-M1
Manufacturer: INSTITUTE OF CHEMISTRY, CAS
Date of Test: 08/11/2022
Temperature Sensor/Control System: None
Environmental conditions: (25±1) C°, RH (57±2) %
Mask: An aperture area of 6.169 mm² (M1#, Certificate No.: CDjc2019-6589)

The test has been conducted by the PV Metrology Lab of NIM (National Institute of Metrology, China). Measurement of irradiance intensity and all other measurements are traceable to the International System of Units (SI). Data in this report apply only at the time of the test for the sample. For more details, please refer to the text of the report.

Forward Scan:

Area (mm^2)	I_{sc}(mA)	V_{oc}(V)	P_{max}(mW)
6.169	1.486	0.937	1.084
I_{max}(mA)	V_{max}(V)	FF (%)	η (%)
1.355	0.800	77.9	17.6

I-V Characterization Methods:
JJF 1622-2017: Calibration Specification of Solar Cells：Photoelectric Properties
Reference Solar Cell:
Type: Mono-Si
Solar Simulator:
Classification: A+AA+ (Double-light source: Xeon and Halogen; IEC 60904-9 2020);
Total irradiance: 1000 W/m² based on I_{sc} of the above Reference Solar Cell.

Report No.: GXgf2022-02337
DUT S/N: 40-M1

I-V Characteristic curves and parameters (Forward Scan)

Steady-state scanning curve (V_{bias} = 0.800 V, $t_{scanning}$ = 300 s, P_{start}= 1.082 mW and P_{finish}= 1.052 mW)

Figure S7. I-V and the steady-state scanning curve of the certificate from NIM, China.

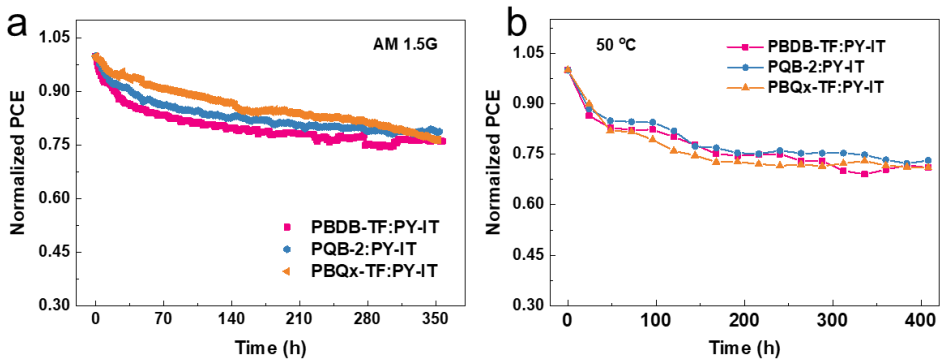

Figure S8. The stability of devices under (a) light irradiation (simulated one-sun intensity using a LED array) and (b) thermal annealing (50 °C) conditions.

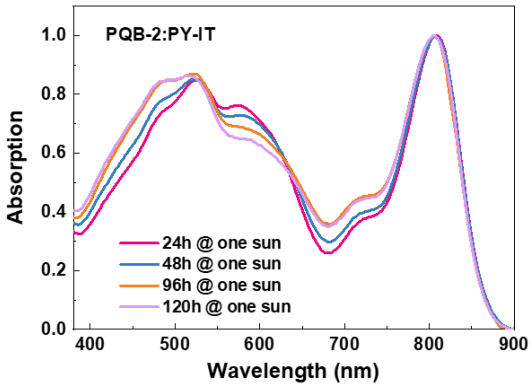

Figure S9. The absorption spectra of PQB-2:PY-IT film under light irradiation (simulated one-sun intensity using a LED array) conditions.

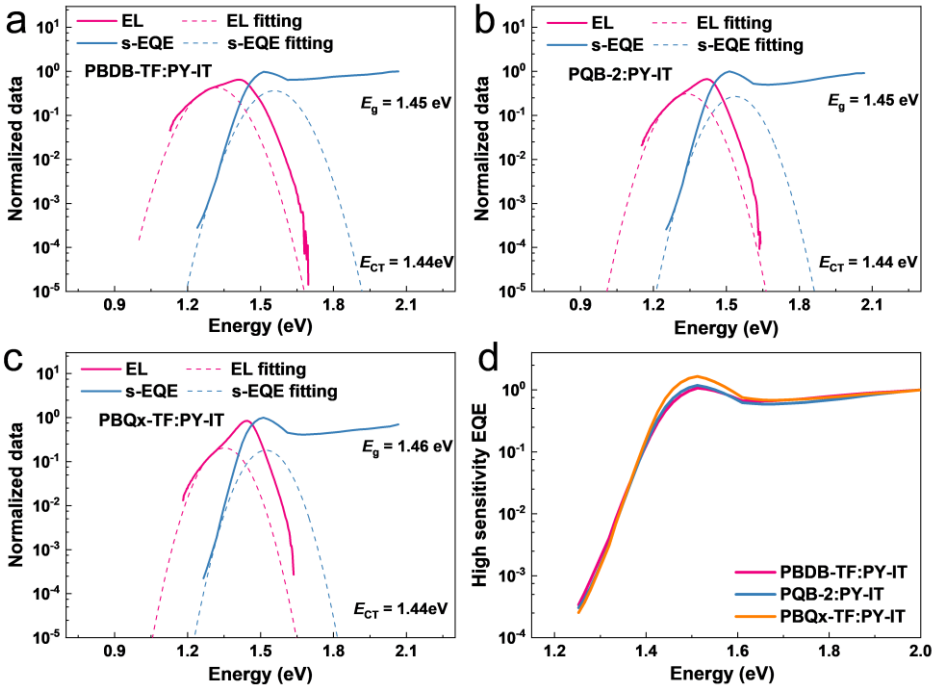

Figure S10. EL and highly sensitive EQE (s-EQE) and their fitted curves of (a) PBDB-TF-TF:PY-IT, (b) PQB-2:PY-IT, and (c) PBQx-TF:PY-IT-based PSCs. (d) highly sensitive EQE (s-EQE) of all PSCs.

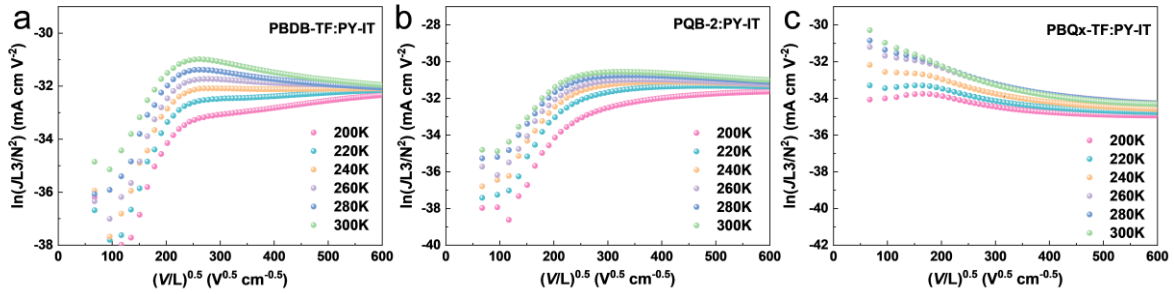

Figure S11. SCLC plots under different temperatures for (a) PBDB-TF:PY-IT, (b) PQB-2:PY-IT, and (c) PBQx-TF:PY-IT-based devices.

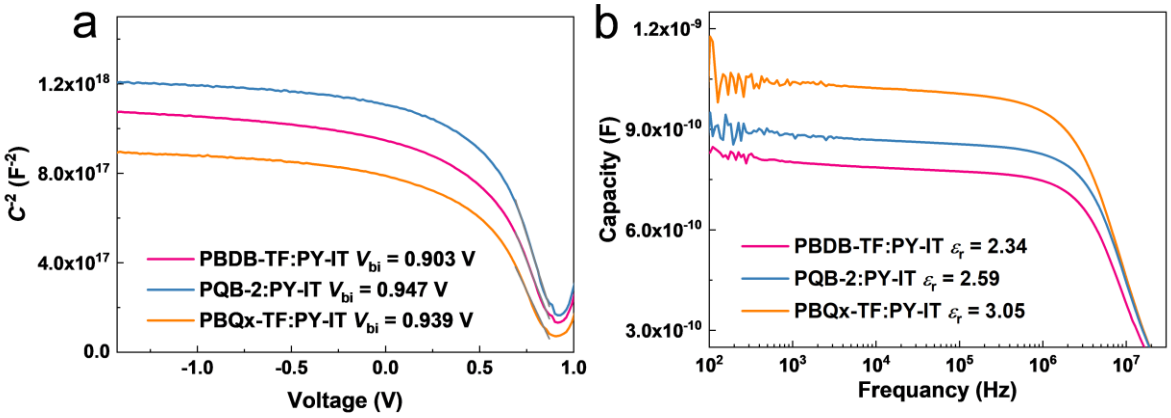

Figure S12. The (a) built-in potential and (b) capacity-frequency spectra of PBDB-TF:PY-IT, PQB-2:PY-IT and PBQx-TF:PY-IT.

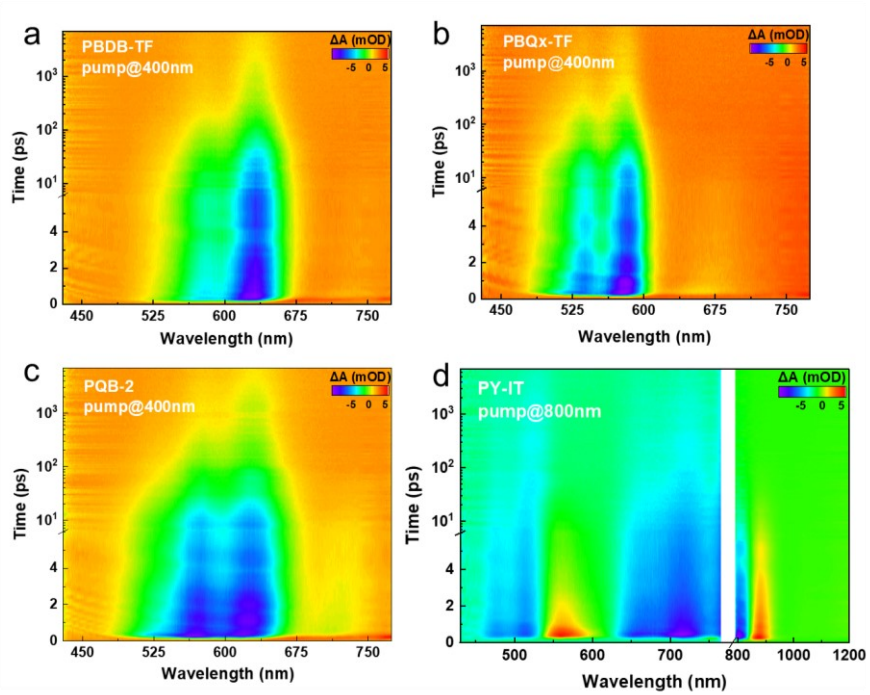

Figure S13. 2D TA profiles of neat (a) PBDB-TF, (b) PBQx-TF, (c) PQB-2, and (d) PY-IT films.

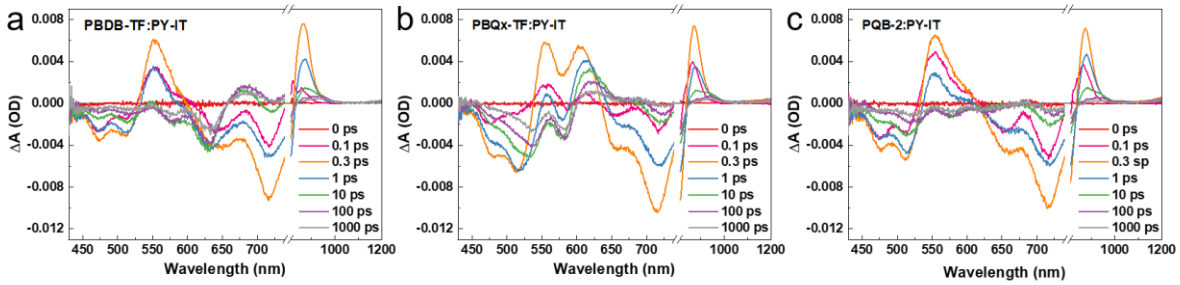

Figure S14. TA spectra at various delay times of PBDB-TF:PY-IT, PBQx-TF:PY-IT and PQB-2:PY-IT films.

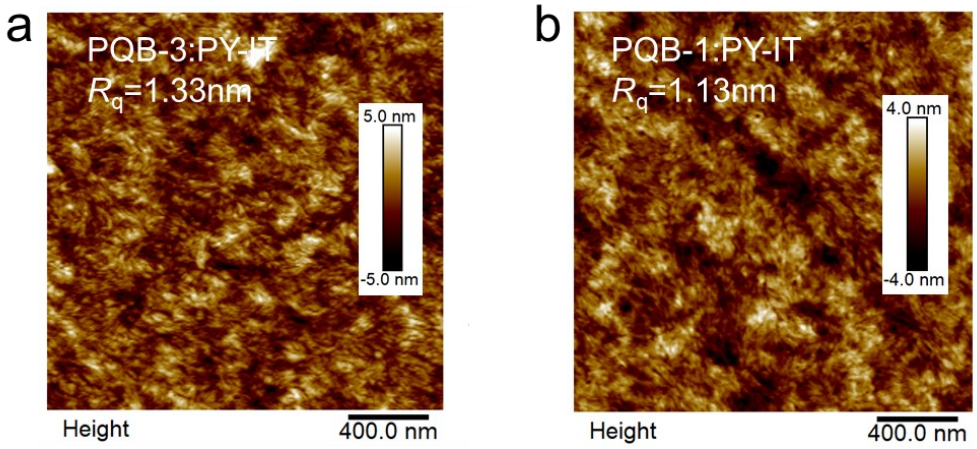

Figure S15. AFM height images of the (a) PQB-3:PY-IT and (c) PQB-1: PY-IT-based films.

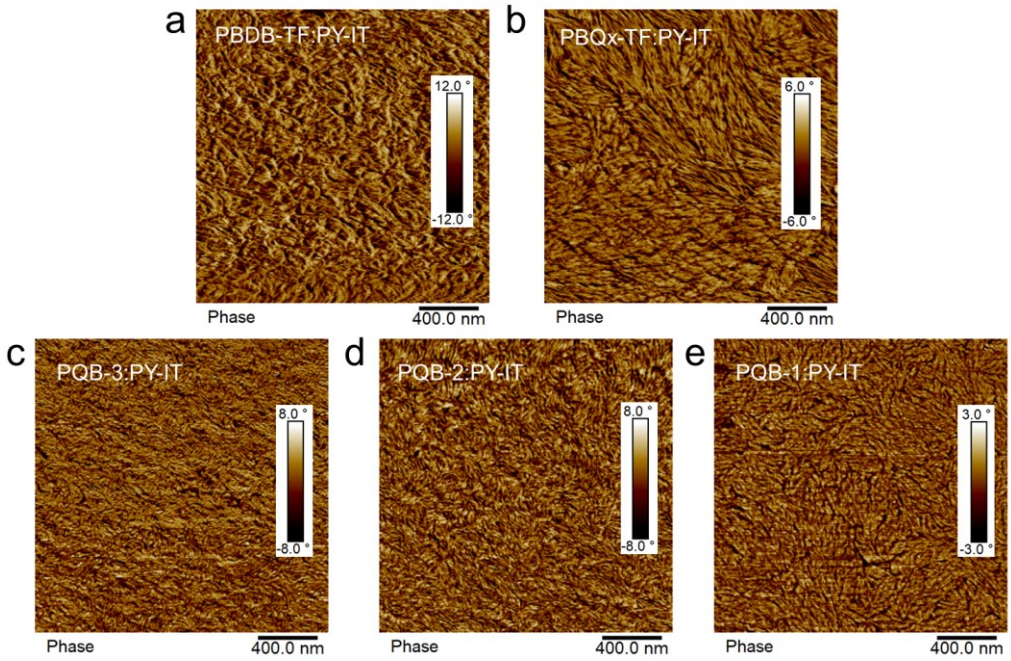

Figure S16. AFM phase images of all polymer:PY-IT-based films.

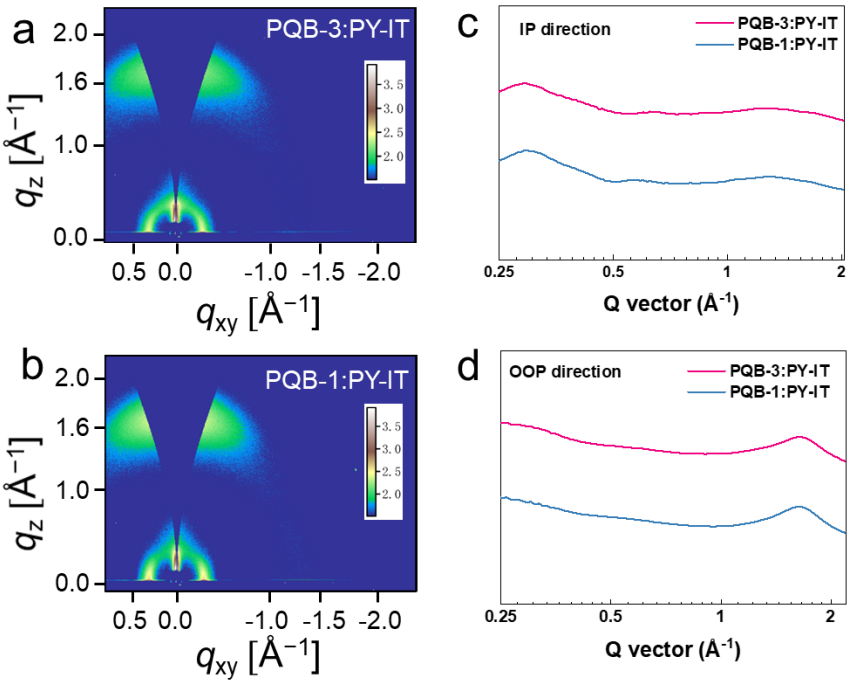

Figure S17. (a,b) 2D-GIWAXS patterns of PQB-3:PY-IT and PQB-1:PY-IT films. (c,d) The GIWAXS profiles of PQB-3:PY-IT and PQB-1:PY-IT films in IP and OOP directions.

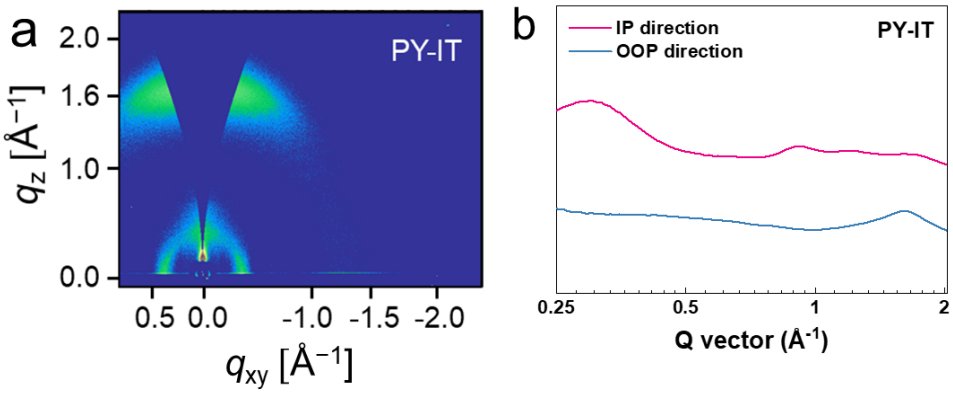

Figure S18. (a) Two-dimensional GIWAXS pattern and (b) GIWAXS profiles of PY-IT film.

Table S1. Summary of photovoltaic parameters of the state of the art all-PSCs.

System	V_{OC} (V)	J_{SC} (mA cm^{-2})	FF (%)	PCE (%)	Ref.
PBDB-T:PY-T	0.91	23.07	77.0	16.05	[3]
PM6:PY-IT:BN-T	0.96	22.65	74.3	16.09	[4]
PM6:PY2Se-Cl	0.884	24.5	74.3	16.1	[5]
JD40:PJTVT	0.89	23.75	76.4	16.13	[6]
PM6:PYT-1S1Se	0.926	24.1	73	16.3	[7]
PM6:PY-V-γ	0.912	24.8	75.8	17.1	[8]
PM6:PYT:PY2F-T	0.904	25.05	76.02	17.22	[9]
PBQx-TCl:PY-IT	0.920	24.3	80.7	18.0	[10]

Table S2. The detailed photovoltaic parameters of all-PSCs.

Active layer	V_{OC} (V)	J_{SC} (mA cm^{-2})	FF	PCE (%)
PBQx-TF:PY-IT	0.917	23.6	0.796	17.2 (16.9 ± 0.2)
PQB-1:PY-IT	0.930	23.8	0.791	17.5 (17.1 ± 0.3)
PQB-2:PY-IT	0.942	24.2	0.795	18.1 (17.8 ± 0.2)
PQB-3:PY-IT	0.940	23.8	0.766	17.1 (16.9 ± 0.2)
PBDB-TF:PY-IT	0.938	23.5	0.729	16.1 (15.9 ± 0.2)

Table S3. The detailed photovoltaic parameters of different thickness PQB-2:PY-IT-based PSCs.

Thickness (nm)	V_{OC} (V)	J_{SC} (mA cm^{-2})	FF	PCE (%) [(a)]
100 ± 10	0.942	24.2	0.795	18.1 (17.8 ± 0.2)
150 ± 10	0.936	24.3	0.766	17.4 (17.1 ± 0.2)
250 ± 10	0.931	25.1	0.715	16.7 (16.4 ± 0.2)
350 ± 10	0.919	25.0	0.674	15.5 (15.3 ± 0.2)

Table S4. The standard deviation of mobility and hole disorder for polymer and polymer:PY-IT films.

	PBDB-TF	PQB-2	PBQx-TF	PBDB-TF:PY-IT	PQB-2:PY-IT	PBQx-TF:PY-IT
Mobility (10^{-4} cm^2 V^{-1} s^{-1})	1.75 (1.65±0.18)	1.38 (1.13±0.21)	0.94 (0.92±0.19)	1.15 (1.05±0.10)	2.30 (2.05±0.21)	1.1 (1.01±0.11)
Hole disorder (meV)	53 (53.6±1.1)	44 (44.4±1.5)	47 (47.2±1.3)	45 (45.6±0.5)	36 (37.0±1.1)	42 (43.1±0.9)

References

1. D. Qian, L. Ye, M. Zhang, Y. Liang, L. Li, Y. Huang, X. Guo, S. Zhang, Z. a. Tan and J. Hou, *Macromolecules*, 2012, **45**, 9611-9617.
2. Y. Xu, Y. Cui, H. Yao, T. Zhang, J. Zhang, L. Ma, J. Wang, Z. Wei and J. Hou, *Adv. Mater.,* 2021, **33**, 2101090.
3. Y. Zhang, B. Wu, Y. He, W. Deng, J. Li, J. Li, N. Qiao, Y. Xing, X. Yuan, N. Li, C. J. Brabec, H. Wu, G. Lu, C. Duan, F. Huang and Y. Cao, *Nano Energy*, 2022, **93**, 106858.
4. T. Liu, T. Yang, R. Ma, L. Zhan, Z. Luo, G. Zhang, Y. Li, K. Gao, Y. Xiao, J. Yu, X. Zou, H. Sun, M. Zhang, T. A. Dela Peña, Z. Xing, H. Liu, X. Li, G. Li, J. Huang, C. Duan, K. S. Wong, X. Lu, X. Guo, F. Gao, H. Chen, F. Huang, Y. Li, Y. Li, Y. Cao, B. Tang and H. Yan, *Joule*, 2021, **5**, 914-930.
5. Q. Fan, H. Fu, Z. Luo, J. Oh, B. Fan, F. Lin, C. Yang and A. K. Y. Jen, *Nano Energy*, 2022, **92**, 106718.
6. J. Zhang, C. H. Tan, K. Zhang, T. Jia, Y. Cui, W. Deng, X. Liao, H. Wu, Q. Xu, F. Huang and Y. Cao, *Adv. Energy Mater.*, 2021, **11**, 2102559.
7. H. Fu, Q. Fan, W. Gao, J. Oh, Y. Li, F. Lin, F. Qi, C. Yang, T. J. Marks and A. K. Y. Jen, *Sci. China Chem.*, 2021, **65**, 309-317.
8. H. Yu, Y. Wang, H. K. Kim, X. Wu, Y. Li, Z. Yao, M. Pan, X. Zou, J. Zhang, S. Chen, D. Zhao, F. Huang, X. Lu, Z. Zhu and H. Yan, *Adv. Mater.*, 2022, **34**, 2200361.
9. R. Sun, W. Wang, H. Yu, Z. Chen, X. Xia, H. Shen, J. Guo, M. Shi, Y. Zheng, Y. Wu, W. Yang, T. Wang, Q. Wu, Y. Yang, X. Lu, J. Xia, C. J. Brabec, H. Yan, Y. Li and J. Min, *Joule*, 2021, **5**, 1548-1565.
10. J. Wang, Y. Cui, Y. Xu, K. Xian, P. Bi, Z. Chen, K. Zhou, L. Ma, T. Zhang, Y. Yang, Y. Zu, H. Yao, X. Hao, L. Ye and J. Hou, *Adv. Mater.*, 2022, **34**, 2205009.